The potential energy surface of He–HCN determined by fitting to highresolution spectroscopic data

Keith M. Atkins and Jeremy M. Hutson

Citation: The Journal of Chemical Physics **105**, 440 (1996); doi: 10.1063/1.471897
View online: http://dx.doi.org/10.1063/1.471897
View Table of Contents: http://scitation.aip.org/content/aip/journal/jcp/105/2?ver=pdfcov
Published by the AIP Publishing

The potential energy surface of He–HCN determined by fitting to high-resolution spectroscopic data

Keith M. Atkins and Jeremy M. Hutson
Department of Chemistry, University of Durham, South Road, Durham, DH1 3LE, England

(Received 9 February 1996; accepted 4 April 1996)

Two potential energy surfaces for He–HCN are determined by least-squares fitting of parameterised functional forms to data from high-resolution microwave and millimeter-wave spectroscopy [Drucker *et al.*, J. Phys. Chem. **99**, 2646 (1995)]. The two potentials both have significantly deeper wells than suggested by the *ab initio* supermolecule calculations of Drucker *et al.* Both potentials have linear or near-linear equilibrium geometries, He–H–C–N, but the shapes of the well depth functions away from the linear geometry are significantly different. The existing experimental data are thus not sufficient to probe this potential feature in detail. Predictions of spectroscopic properties that would allow the new potentials to be tested and refined are given. © *1996 American Institute of Physics.* [S0021-9606(96)01926-5]

I. INTRODUCTION

The spectra of van der Waals complexes contain detailed information on intermolecular forces. Over the last 10 or 15 years, high-resolution microwave and infrared spectra have been used to determine complete potential energy surfaces for a variety of prototype atom–molecule systems including Ar–H_2,[1] Ar–HF,[2] Ar–HCl,[3] Ar–H_2O[4] and Ar–NH_3.[5] These systems contain hydride monomers with low moments of inertia, which execute very wide amplitude angular motions in the complex, so that the spectra are sensitive to the potential at the full range of angular geometries. Although high-resolution spectra have also been used to obtain potential energy surfaces for heavier atom–molecule systems such as Ar–CO_2[6] and for light molecule–molecule systems such as HF–HF[7] and HCl–HCl,[8] for these complexes the angular motions are more confined and the spectra are sensitive to a smaller part of the complete potential energy surface: The quality of the resulting potential then depends strongly on the functional forms used to extrapolate the potential into the unsampled regions.

Complexes containing He are much more weakly bound than those containing heavier rare gas atoms, so that He complexes execute wide-amplitude bending motions even when they contain monomers with larger moments of inertia. However, because of the weak binding, He complexes are much more difficult to form than Ar complexes: In jets and molecular beams, they typically require cooled nozzles and very low concentrations of the non-He partner. Until recently, most of the information available on potential energy surfaces involving He came from crossed molecular beam scattering experiments.

Over the last five years, it has become possible to observe the infrared spectra of He complexes in molecular beams by laser absorption spectroscopy. Species studied in this way have included He–HF,[9] He–HCl[9] and He–CO_2.[10] In addition, complexes such as He–CO[11] have been observed in low-temperature gas mixtures by Fourier transform infrared spectroscopy. These spectra have been used to test various intermolecular potentials,[10,12] but for the most part the data have not been extensive enough to fit a potential energy surface directly to the experimental results.

Recently, Drucker *et al.*[13] reported microwave and millimeter-wave spectra of the He–HCN complex, together with preliminary *ab initio* calculations of the He–HCN potential surface. He–HCN is of particular interest for two reasons: First, HCN has a much stronger repulsive anisotropy than molecules such as HF and HCl, in which the H atom is largely buried in the near-spherical charge cloud of the halogen atom. He–HCN thus provides a prototype system in which a rod-like molecule executes very wide-amplitude motions. Second, the spectra of Drucker *et al.* are at high enough resolution to determine nuclear quadrupole coupling constants for the ^{14}N nucleus, which contain valuable additional information on the angular wave functions of the complex and thus on the anisotropy of the potential. The availability of the nuclear quadrupole coupling constants for He–HCN provides enough additional information to make it feasible to fit a potential energy surface for this system.

For van der Waals complexes such as Ar–HCl or Ar–HCN, it is usual to interpret nuclear quadrupole coupling constants in terms of angular expectation values. For example, since the a inertial axis of the complex usually lies very close to the intermolecular vector R, and the quadrupole coupling constant is a second-rank tensor, the aa component of the coupling constant of the complex is usually assumed to be given by

$$(eqQ)_{aa}=(eqQ)_{\mathrm{monomer}}\langle P_2(\cos\theta)\rangle, \tag{1}$$

where θ is the angle between the HCN vector and the R vector, measured at the monomer center of mass, and $P_2(\cos\theta)$ is the second Legendre polynomial. However, for complexes containing molecules with large moments of inertia with light atomic or molecular partners, it is no longer an adequate approximation to assume that the a axis lies along the R vector, or even to consider the projection onto the instantaneous principal axes.[14] For complexes such as Ar–CO_2 that exhibit low-amplitude bending motions, it is necessary to consider the projection onto Eckart axes that

 0021-9606/96/105(2)/440/11/$10.00

move as the complex vibrates. However, for complexes where complete internal rotation is feasible, even the Eckart axes break down. Under these circumstances, it is necessary to consider the interaction between the nuclear quadrupole moment and the electric field gradient explicitly.[15] He–HCN, which contains both a monomer with two heavy atoms and a very light partner, is an excellent example of a complex that requires the full treatment.

The purpose of the present paper is to describe potential energy surfaces that we have fitted to the spectroscopic data for He–HCN. The structure of the paper is as follows. Section II describes the functional forms that we have used for the potentials. Section III describes the spectroscopic data used in the fits. Section IV describes the fitting of potential energy surfaces to both *ab initio* points and spectroscopic data. Section V describes some important features of the final potential energy surfaces, and Section VI summarizes our conclusions.

Throughout this work we have assumed that the HCN monomer behaves as though it was a rigid rotor. The potentials that we obtain are thus effective two-dimensional potentials, adiabatically averaged over the internal vibrational motions of the HCN molecule in its ground vibrational state. The coordinates used are R, the distance from the He atom to the HCN center of mass, and θ, the angle between the He to HCN center of mass vector and the axis of the HCN monomer, where $\theta=0$ corresponds to the linear configuration He–HCN.

II. FUNCTIONAL FORMS FOR THE POTENTIAL ENERGY SURFACES

In the present work, we have used two quite different functional forms for the potential energy surface. However, both of them may be represented in the general form

$$V(R,\theta)=V^{\text{rep}}+V^{\text{ind}}+V^{\text{disp}}, \tag{2}$$

where the three terms represent the intermolecular repulsion, induction and dispersion. Both potential forms are constrained to have R^{-6} and R^{-7} terms that correctly represent the induction and dispersion forces at long range. We will therefore describe these long-range terms first.

The induction energy for an atom + linear molecule system is given to order R^{-7} by[16]

$$V^{\text{ind}}=-\alpha_{\text{He}}\mu_{\text{HCN}}^2[1+P_2(\cos\ \theta)]R^{-6} -6\alpha_{\text{He}}\mu_{\text{HCN}}\Theta_{\text{HCN}}\cos^3\ \theta R^{-7}, \tag{3}$$

where $\alpha_{\text{He}}=1.383\ a_0^3$ is the static dipole polarizability of He and $\mu_{\text{HCN}}=1.174\ ea_0$ and $\Theta_{\text{HCN}}=1.777\ ea_0^2$ are the dipole[17] and quadrupole[18] moments of HCN.

In a single-site representation, the dispersion part of the potential (neglecting damping, which will be considered later) may be expanded

$$V^{\text{disp}}=-\sum_{n=6}^{8} C_n(\theta)R^{-n}, \tag{4}$$

where the leading terms are

TABLE I. Dispersion coefficients (in atomic units).

	Our values	Drucker *et al.*[a]
$C_6^{(0)}$	13.067	19.4
$C_6^{(2)}$	1.864	0.342
$C_7^{(1)}$	9.939	16.99
$C_7^{(3)}$	9.401	−1.15

[a]Drucker *et al.* expand the C_7 terms as a Legendre expansion. Here we have converted their expansion to the polynomial form used in this work.

$$C_6(\theta)=C_6^{(0)}+C_6^{(2)}P_2(\cos\ \theta) \tag{5}$$

and

$$C_7(\theta)=C_7^{(1)}\cos\ \theta+C_7^{(3)}\cos^3\ \theta. \tag{6}$$

The coefficients may be expressed in terms of the parallel and perpendicular components of the dipole–dipole polarizabilities α and dipole–quadrupole polarizabilities A at imaginary frequencies,[19]

$$C_6^{(0)}=\frac{1}{\pi}\int_0^\infty \alpha_{\text{He}}(i\omega)(\alpha^{\parallel}_{\text{HCN}}(i\omega)+2\alpha^{\perp}_{\text{HCN}}(i\omega))\ \mathrm{d}\omega; \tag{7}$$

$$C_6^{(2)}=\frac{1}{\pi}\int_0^\infty \alpha_{\text{He}}(i\omega)(\alpha^{\parallel}_{\text{HCN}}(i\omega)-\alpha^{\perp}_{\text{HCN}}(i\omega))\ \mathrm{d}\omega; \tag{8}$$

$$C_7^{(1)}=\frac{1}{\pi}\int_0^\infty 12\alpha_{\text{He}}(i\omega)A^{\perp}_{\text{HCN}}(i\omega)\ \mathrm{d}\omega; \tag{9}$$

$$C_7^{(3)}=\frac{1}{\pi}\int_0^\infty \alpha_{\text{He}}(i\omega)(6A^{\parallel}_{\text{HCN}}(i\omega)-8A^{\perp}_{\text{HCN}}(i\omega))\ \mathrm{d}\omega. \tag{10}$$

To evaluate the dispersion coefficients in the present work, we carried out coupled Hartree–Fock (CHF) *ab initio* calculations of the frequency-dependent polarizabilities for HCN. The calculations were carried out using the CADPAC[20] program, with uncontracted $8s6p3d$ basis sets for the N and C atoms and a $6s3p$ basis set for the H atom. The bond lengths used were $r_{\text{CN}}=2.1845\ a_0$ and $r_{\text{CH}}=2.0107\ a_0$. The static HCN polarizabilities from this calculation are $\alpha^{\parallel}_{\text{HCN}}=22.485\ a_0^3$ and $\alpha^{\perp}_{\text{HCN}}=12.985\ a_0^3$, in reasonable agreement with the estimates of the Hartree–Fock limit given by Fowler and Diercksen,[21] which are 22.5 and 13.8 a_0^3 respectively. The results of Fowler and Diercksen suggest that the correlation contributions to the polarizabilities are less than about 0.5 a_0^3 for HCN.

Values of $\alpha_{\text{He}}(i\omega)$ were taken from the work of Koide *et al.*[22] The integrals over imaginary frequency were performed using the midpoint quadrature scheme of Koide *et al.*, with 30 quadrature points. The resulting values of the dispersion coefficients are given in Table I.

A. Form 1

The first potential form that we consider is the same as the H6 functional form previously used for various rare gas + hydrogen halide systems.[23–25] The short-range repulsion is a simple exponential at each angle,

$$V^{\mathrm{rep}} = A(\theta)\exp(-\beta R). \tag{11}$$

The induction energy is represented directly as in Eq. (3), without damping. The dispersion energy is represented as a single-center expansion about the HCN center of mass,

$$V^{\mathrm{disp}} = -\sum_{n=6}^{8} C_n(\theta) D_n(R) R^{-n}, \tag{12}$$

where the functions $D_n(R)$ are Tang–Toennies damping functions,[26]

$$D_n(R) = 1 - \exp(-\beta R)\sum_{m=0}^{n} \frac{(\beta R)^m}{m!}. \tag{13}$$

It may be noted that, since β is assumed to be independent of θ, these damping functions are independent of angle. This is a reasonable approximation for the rare gas + hydrogen halide systems, but is perhaps questionable for He–HCN. The coefficients $C_6(\theta)$ and $C_7(\theta)$ and the parameters of the induction energy are fixed on the basis of monomer properties as described above. The quantities $A(\theta)$, β and $C_8(\theta)$ are adjustable, and could be expanded in Legendre series to obtain a set of fittable parameters. However, when fitting to experimental data, it has usually been found that fitting directly to parameter sets governing the attractive and repulsive parts of the potential gives a highly correlated fit, with parameters that are poorly determined. Instead, it is generally better to expand the depth, ϵ, and position, R_m, of the energy minimum as Legendre series,

$$\epsilon(\theta) = \sum_{\lambda} \epsilon_\lambda P_\lambda(\cos\theta); \tag{14}$$

$$R_m(\theta) = \sum_{\lambda} R_{m\lambda} P_\lambda(\cos\theta). \tag{15}$$

It is then straightforward to obtain values of $A(\theta)$ and $C_8(\theta)$ from the other parameters at each value of θ, as described in Appendix 1 of Ref. 23. It should be noted that the coefficient $C_8(\theta)$ obtained in this way represents not only the true C_8 dispersion term, but also all other terms that have otherwise been neglected. This can give rise to a C_8 term that is larger and more anisotropic than the true dispersion C_8 term.

B. Form 2

For the second potential form, we use a more sophisticated representation of the repulsion, based on the overlap of the monomer charge densities, and also distribute the dispersion interaction between two sites in the HCN molecule.

The repulsion potential is assumed to be proportional to the charge density overlap of the two monomers,

$$V^{\mathrm{rep}}(R,\theta) = K_\rho S_\rho(R,\theta), \tag{16}$$

where

$$S_\rho(R,\theta) = \int \rho_{\mathrm{He}} \rho_{\mathrm{HCN}}\, \mathrm{d}\tau. \tag{17}$$

This approximation has been found to hold well for a variety of systems:[27] It allows the shape and hardness of the repulsive wall to be built in without the expense of supermolecule calculations. In the present work, we carried out Møller–Plesset (MP2) calculations of the monomer electron densities, using the CADPAC program.[20] The HCN basis set was the same as described above ($8s6p3d$ basis sets for N and C and $6s3p$ for H), with a $16s8p4d$ basis set for He. The charge density overlap integrals were then calculated using the GMUL program.[28] Initially, we used an option within GMUL that decomposed the overlap into a sum of anisotropic site–site interactions, with two or three sites located along the HCN axis. However, we found that the parameters required to fit the individual site–site interactions were in some respects unsatisfactory (for example, some of the anisotropic terms required longer-ranged exponentials than the isotropic terms, and so would dominate unphysically at long range). This probably reflects the fact that the assignment of individual orbital overlap contributions to particular sites within the GMUL program is somewhat arbitrary. We therefore ultimately chose to evaluate the function $S_\rho(R,\theta)$ at a grid of points formed by the 10 Gauss–Legendre quadrature angles and a set of 11 evenly distributed R values between 6 and 12 a_0. The resulting values were then fitted to the functional form

$$S_\rho(R,\theta) = A\,\exp[-\beta(\theta)(R - R_w(\theta))], \tag{18}$$

where A is fixed (at 1 a.u.) and $\beta(\theta)$ and $R_w(\theta)$ are each expanded in Legendre polynomials,

$$\beta(\theta) = \sum_{\lambda} \beta_\lambda P_\lambda(\cos\theta); \tag{19}$$

$$R_w(\theta) = \sum_{\lambda} R_{w\lambda} P_\lambda(\cos\theta). \tag{20}$$

The optimum values of β_λ and $R_{w\lambda}$ were determined by least-squares fitting using routine E04FDF from the NAG FORTRAN library.[29] In order to obtain the best representation of the overlap function in the most important region, which is the lower part of the repulsive wall of the potential, the fit was weighted with a weighting function chosen to be a Gaussian in $\ln S_\rho$, with unit width and the center corresponding to repulsion energies of about 100 cm^{-1}.

Both the Legendre expansions were carried out including terms up to $\lambda_{\max} = 9$. The resulting parameters are given in Table II, and the corresponding functions $\beta(\theta)$ and $R_w(\theta)$ are shown in Figure 1.

The single-center dispersion expansion (12) is satisfactory for small molecules, but becomes poorly convergent at intermolecular distances small enough to be comparable to the size of one of the monomers. Even for systems such as Ar–HF and Ar–HCl, Douketis *et al.*[30] found that it was advantageous to split the dispersion into two sites, with one site at the center of mass and the other half-way along the H–X bond. For HCN, we choose to use two dispersion centers located along the axis of the molecule. The positions of the two sites are expressed as displacements δ_{A} and δ_{B} from the HCN center of mass. The potential is thus written,

TABLE II. Legendre coefficients in expansion of β and R_w for potential 2.

Legendre component, λ	β_λ (a_0^{-1})	$R_{w\lambda}$ (a_0)
0	2.0486	1.4380
1	0.0422	0.2181
2	0.1434	1.0737
3	0.0537	0.2233
4	0.0123	0.0735
5	0.0016	0.0434
6	−0.0029	−0.0039
7	−0.0055	−0.0228
8	−0.0025	−0.0101
9	−0.0009	−0.0027

$$V^{\rm disp}(R,\theta)=\sum_{\rm X=A,B}\sum_{n=6,8,10} C_{{\rm X}n}(\theta_{\rm X})D_n(R_{\rm X})R_{\rm X}^{-n}, \tag{21}$$

where $R_{\rm X}$ and $\theta_{\rm X}$ are the coordinates with respect to the dispersion sites.

Each site–site coefficient $C_6(\theta)$ is of the form

$$C_6(\theta)=C_6^{(0)}+C_6^{(2)}P_2(\cos\,\theta). \tag{22}$$

As described for potential form 1, we obtain values for the coefficients $C_6^{(0)}$, $C_6^{(2)}$, $C_7^{(1)}$ and $C_7^{(3)}$ for a single-site expansion about the monomer center of mass from *ab initio* calculations. The dispersion coefficients on the two sites are chosen to maintain these overall values for the R^{-6} and R^{-7} terms. Expanding the coordinates $R_{\rm X}$ and $\theta_{\rm X}$ in terms of R and θ gives

$$C_6^{(0)}=C_{\rm A6}^{(0)}+C_{\rm B6}^{(0)};$$

$$C_6^{(2)}=C_{\rm A6}^{(2)}+C_{\rm B6}^{(2)};$$

$$C_7^{(1)}=6\delta_{\rm A}[C_{\rm A6}^{(0)}-C_{\rm A6}^{(2)}]+6\delta_{\rm B}[C_{\rm B6}^{(0)}-C_{\rm B6}^{(2)}];$$

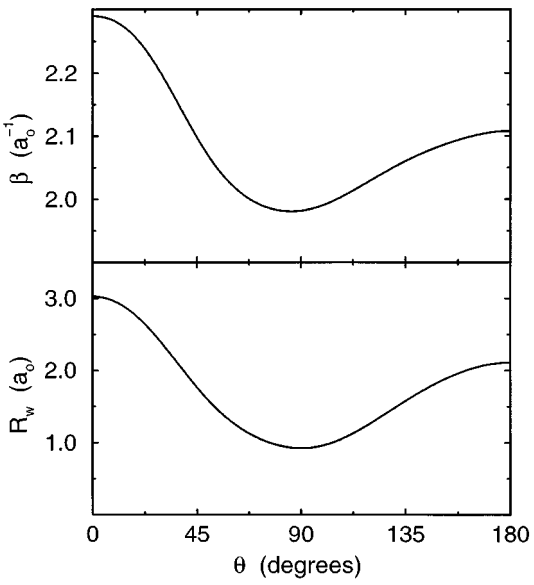

FIG. 1. The functions $\beta(\theta)$ and $R_w(\theta)$ describing the charge density overlap of the He and HCN [see Eq. (18)].

$$C_7^{(3)}=12\delta_{\rm A}C_{\rm A6}^{(2)}+12\delta_{\rm B}C_{\rm B6}^{(2)}. \tag{23}$$

These four equations uniquely define $C_{\rm X6}^{(0)}$ and $C_{\rm X6}^{(2)}$ on both sites for given $\delta_{\rm A}$ and $\delta_{\rm B}$ in terms of the overall C_6 and C_7 coefficients. Flexibility is introduced into the potential through the higher-order coefficients. The Legendre coefficients of $C_8(\theta_{\rm X})$ are expressed in terms of those of $C_6(\theta_{\rm X})$,

$$C_{\rm X8}^{(\lambda)}=\tau_{\rm X}^{(\lambda)}C_{\rm X6}^{(\lambda)}. \tag{24}$$

In this work we set $\tau_{\rm X}^{(2)}=\tau_{\rm X}^{(0)}=\tau_{\rm X}$.

Coefficients $C_{\rm X10}^{(n)}$ are included for completeness. In the present work, we set

$$C_{\rm X10}(\theta_{\rm X})=\frac{49}{40}\frac{C_{\rm X8}(\theta_{\rm X})}{C_{\rm X6}(\theta_{\rm X})}, \tag{25}$$

although additional flexibility could be introduced here if necessary.

We again use the Tang–Toennies damping functions, Eq. (13), with the distance scaling factor set to the zeroth term in the Legendre expansion of $\beta(\theta)$ [β_0 in Eq. (18)].

III. THE SPECTROSCOPIC DATA

The energy levels of a weakly anisotropic atom–molecule complex such as He–HCN are best described in a case 1 (''space-fixed'') coupling scheme.[31] The rotational quantum number j of the HCN monomer is nearly conserved in the complex. In He–HCN, the anisotropy of the potential is too weak to overcome the rotational coupling, so that j is not quantised along the intermolecular vector R to give a projection quantum number K. Instead, j couples to L, the quantum number for rotation of He and HCN about their center of mass, to form J, the total angular momentum neglecting nuclear spin. For given values of j and L, J can take values from $|j-L|$ to $j+L$: The different J levels are weakly split by the potential anisotropy, but the splitting is small compared to that between levels of different L (or j).

The parity of a rotational level is $(-1)^{j+L}$, and must change in a dipole-allowed transition.

Drucker *et al.*[13] measured three millimeter-wave lines of He–HCN, near 101.2, 101.4, and 105.8 GHz. These lines all involve rotational excitation $j=1\leftarrow 0$ of the HCN molecule in the complex. Drucker *et al.* resolved the hyperfine structure of the stronger lines, at 101.4 and 105.8 GHz lines. In addition, they measured three microwave lines, around 15.9, 31.1, and 31.3 GHz, with their hyperfine structure, in double resonance with the millimeter-wave lines. From a consideration of the double-resonance results and the observed hyperfine structure, the microwave lines at 15.9 and 31.3 GHz were assigned to the $J=1\leftarrow 0$ and $2\leftarrow 1$ transitions in the ground state: In case 1 notation, these are the $(j,L,J)=(0,1,1)\leftarrow(0,0,0)$ and $(0,2,2)\leftarrow(0,1,1)$ transitions. Because of the strong coupling between the bending vibration (or internal rotation of HCN in the complex) and the end-over-end rotational motion, a separate nuclear quadrupole coupling constant eq_JQ was needed for each rotational

TABLE III. Fitted parameters for the potential of Drucker *et al.* and our potentials 1*A*8 and 1*E*8.

Parameter	Drucker *et al.*	1*A*	1*E*8
ϵ_0 (cm^{-1})	19.3	19.399	24.825(139)
ϵ_1 (cm^{-1})	3.49	3.402	3.402
ϵ_2 (cm^{-1})	1.47	1.407	0.385(3)
ϵ_3 (cm^{-1})	0.973	0.854	0.854
β (Å $^{-1}$)	4.78	4.265	3.901(15)
R_{m0} (Å)	3.79	3.797	3.715(1)
R_{m1} (Å)	0.0192	0.020	0.200
R_{m2} (Å)	0.395	0.395	0.458(2)
R_{m3} (Å)	0.065	0.071	0.071

level.[32] Drucker *et al.* obtained $eq_JQ=0.1118(15)$ MHz for the $J=1$ level and 0.199(12) MHz for the $J=2$ level.

The double-resonance results establish the identity of the lower states of the millimeter-wave transitions. However, the upper-state assignments are less secure. The 101.4 GHz line originates in the (0,1,1) state: The parity selection rule requires that ΔL is even when Δj is 1, so the upper state could in principle be (1,1,0) [i.e., $P(1)$], (1,1,1) [i.e., $Q(1)$] or (1,1,2) [i.e., $R(1)$]. However, (1,1,0) is excluded by the presence of quadrupole splitting in the upper state. Drucker *et al.* argued for an $R(1)$ assignment on the basis of the quadrupole coupling constant. As will be seen below, our calculations of the quadrupole coupling confirm this assignment. Similarly, the 105.8 GHz line originates in the (0,2,2) state, and might be assigned to $P(2)$, $Q(2)$ or $R(2)$. Drucker *et al.* were not able to assign this line, but our calculations (see below) show that the only plausible assignment is $R(2)$. Similarly, the only plausible assignment for the 101.2 GHz line is $Q(2)$. The 31.1 GHz microwave line is connected to the other frequencies by combination differences, and corresponds to the $(1,2,2)\leftarrow(1,1,2)$ transition within the excited internal rotor state.

IV. FITTED POTENTIAL ENERGY SURFACES

A. Fitting to the *ab initio* calculations

For both potential forms, it was convenient to obtain starting parameters by fitting to the *ab initio* points of Drucker *et al.*,[13] who carried out supermolecular MP4 calculations for 23 configurations of He–HCN. The parameters obtained in this way for our two potential forms are given in Tables III and IV. The two potentials are designated 1*A* and 2*A* respectively (where the *A* indicates that they were fitted to *ab initio* calculations).

TABLE IV. Fitted parameters for potentials 2*A* and 2*E*8.

Parameter	2*A*	2*E*8
K_ρ (a_0^2)	8.341	8.019(297)
τ_A (a_0^2)	14.38	18.30(104)
τ_B (a_0^2)	4.73	11.41(110)
δ_A (a_0)	−0.746	−0.676(17)
δ_B (a_0)	2.381	2.237(38)

It may be noted that Drucker *et al.* carried out their own fit to a functional form quite similar to our form 1,[33] but they allowed the long-range coefficients to be determined from the fit to the *ab initio* points, rather than fixing them at independently determined values. Their parameters for the Legendre components of $\epsilon(\theta)$ and $R_m(\theta)$ are similar to ours, but not identical.

For potential 1*A*, we allowed nine parameters to vary: four Legendre components of the well depth, ϵ_λ, four components of the position of the minimum, $R_{m\lambda}$, and one wall hardness parameter β. For potential 2*A*, only five parameters were varied: the two values of τ_X (the C_8/C_6 ratios), the positions δ_X of the two dispersion sites and the multiplicative factor K_ρ that converts the monomer charge density overlap to a repulsive energy.

The fit of our potential 1*A* to the *ab initio* points is reasonable, albeit slightly worse than the fit to these points using the form of Drucker *et al.* They achieved an r.m.s. discrepancy of 0.26 cm^{-1} between the predicted and *ab initio* results whereas our potential 1*A* gives an r.m.s. discrepancy of 0.31 cm^{-1}. However, we floated only nine parameters whereas they floated 13. The fit of potential 2*A* to the *ab initio* points gives an r.m.s. discrepancy of 0.63 cm^{-1} with just five parameters floating.

B. Computational method for the spectroscopic data

To provide calculated quantities to compare with the experimental results, we have carried out close-coupling calculations[31] of the rovibrational levels of He–HCN using the BOUND program.[34] The program sets up the bound-state Schrödinger equation as a set of coupled differential equations,[35] in a basis set constructed from combinations of HCN free-rotor functions and end-over-end rotational functions of the complex. The close-coupling formulation used here is ''exact,'' in the sense that no dynamical approximations are made except for the neglect of matrix elements that couple different vibrational states of the HCN monomer. All the effects of anharmonicity and intermolecular vibration–rotation coupling are fully included.

The BOUND program provides vibration-rotation energy levels, and it is straightforward to calculate transition frequencies from energy differences. However, when carrying out least-squares fits to experimental data, it is not necessarily best to use the raw transition frequencies directly. Instead, it is often better to use combinations of the transition frequencies that are chosen to be sensitive to particular features or parameters of the potential surface. It must be remembered that, in least-squares terms, fitting to two quantities a and b is by no means the same as fitting to $a+b$ and $a-b$, especially if the sum and difference have different uncertainties.

For He–HCN, this consideration applies particularly to the pure rotational transitions. For a rigid molecule, the $J=1\leftarrow0$ and $J=2\leftarrow1$ frequencies differ by a simple factor of 2: The first transition conveys information on the vibrationally-averaged intermolecular distance, but the second transition contains no extra information. For a weakly

bound complex such as He–HCN, it is the *deviation* from rigid behaviour that conveys information on the anharmonicity, and thus (principally) on the well depth. Rather than considering the $J=1\leftarrow 0$ and $J=2\leftarrow 1$ frequencies directly, it is better to consider one transition frequency (say, $\nu_{1\leftarrow 0}$) and the combination

$$\Delta = 2\nu_{1\leftarrow 0} - \nu_{2\leftarrow 1}. \tag{26}$$

If this quantity is expressed in terms of a conventional centrifugal distortion constant D_J, and higher-order distortion constants are neglected, Δ may be identified with $24D_J$.

A similar consideration applies to the millimeter-wave frequencies. As mentioned above, the 105.8 and 101.2 GHz lines both originate in the $(j,L,J)=(0,2,2)$ state and terminate on the (1,2,3) and (1,2,2) states respectively. The splitting between these two upper states is a direct measure of the potential anisotropy, relatively uncontaminated by other effects, so that it is better to fit to this splitting than to the transition frequencies themselves.

As mentioned above, the nuclear quadrupole coupling constants of He–HCN contain important information on the angular wave functions and thus on the potential anisotropy. Once again, it should be noted that for states with $j \neq 0$ nuclear quadrupole coupling would exist even in the absence of potential anisotropy, and it is really the deviations from the zero-anisotropy values that contain useful information. In the present work, the quadrupole coupling constants were calculated by the method of Ref. 15, which involves explicit evaluation of the expectation value of the quadrupole coupling operator $\mathbf{V}\cdot\mathbf{Q}$ for each vibration–rotation state. The experimental quadrupole coupling constants are expressed as J-dependent quantities eq_JQ.[32] In the notation of Ref. 15,

$$eq_JQ = \left(\frac{2(2J-1)}{(2J+1)(2J+2)(2J+3)}\right)^{\frac{1}{2}} \langle\hat{\Omega}\rangle (eQ)_{\text{monomer}} \tag{27}$$

for each vibration–rotation state, where $\hat{\Omega}$ is an operator whose matrix elements in the space-fixed basis set are given in Ref. 15. The ^{14}N nuclear quadrupole coupling constant in the HCN monomer is -4.709 MHz.[36]

In the present work, the close-coupled equations were set up using a space-fixed basis set including all HCN rotor functions up to $j = 14$. The rotational constant of HCN was taken to be 1.478221834 cm^{-1}, and the reduced mass μ of the complex was taken to be 3.486027 u. The coupled equations were solved using the log-derivative shooting method of Johnson.[35,37] The coupled equations were propagated over the range between $R_{\min} = 2.0$ Å and $R_{\max} = 10.0$ Å with step sizes of 0.10 and 0.05 Å , and the eigenvalues were extrapolated to zero step size using Richardson h^4 extrapolation. These parameters give convergence to better than 10^{-6} cm^{-1} for eigenvalues and 2 kHz for the rotational spacings and the frequency combination used to represent the ground-state centrifugal distortion.

C. Spectroscopic assignments and fits to the experimental data

Before we started fitting, the only completely secure spectroscopic assignments were those for the microwave lines at 15.9 and 31.3 GHz. Drucker *et al.*[13] had tentatively assigned the 101.4 GHz millimeter-wave line as $R(1)$: they rejected the alternative possible assignment, $Q(1)$, because for a planar molecule the $J = 1$ state of even (f) parity should have a quadrupole coupling constant given by

$$eq_JQ(J=1^{fr}) = eqQ_{\text{HCN}}/10 = -0.471 \text{ MHz}, \tag{28}$$

and the experimental value is 0.751 MHz, or about $-0.160eqQ_{\text{HCN}}$. However, it is not entirely clear that this argument is valid for a molecule as fluxional as He–HCN. We therefore began by carrying out calculations using our potentials 1*A* and 2*A*, i.e., both functional forms fitted to the supermolecule calculations of Drucker *et al.* The resulting bound-state energies and quadrupole coupling constants are shown in Figure 2. In particular, it may be seen that close-coupling calculations of eq_JQ for the (1,1,1) level confirm that Eq. (28) is correct (and independent of the intermolecular potential). The value predicted for the (1,1,2) level is 0.801 MHz for this potential. This confirms the assignment of the 101.4 GHz line as $R(1)$. The zero-anisotropy (pure case 1 coupling) prediction for the (1,1,2) level is $-eqQ_{\text{HCN}}/5$, or 0.942 MHz, and the difference between this and the experimental value is another measure of the potential anisotropy.

It may be noted that the two fits to the *ab initio* points give significantly different values for both transition frequencies and some of the quadrupole coupling constants. This is simply a reflection of the difference between the two functional forms, and illustrates the difficulties of fitting potentials to widely-spaced sets of points.

At this stage, there were enough securely assigned experimental data to begin fitting to them. We began with potential form 1. The comparison between the observed quantities and those calculated from the unmodified *ab initio* potential 1*A* is shown in Table V. The calculated rotational splitting is significantly too small, indicating that the equilibrium distance for this potential is too large. The nuclear quadrupole coupling constants show qualitatively the right behaviour, but the agreement with experiment is not quantitative, indicating that that the potential anisotropy needs modification.

The six experimental data (three frequencies and three values of eq_JQ) available at this stage are clearly not enough to determine nine potential parameters. We therefore carried out preliminary fits, adjusting the parameters that are best determined by the experimental data and holding the rest constant at the *ab initio* values. The fits were carried out using the I-NoLLS program,[38] which is an interactive nonlinear least-squares package that allows easy visualisation of highly-correlated parameter spaces and gives the user detailed control over the progress of the fit. After some experimentation, we established that a reasonable fit to this data set could be obtained by adjusting only ϵ_0, ϵ_2 and R_{m0}. How-

FIG. 2. The bound-state energies and quadrupole coupling constants for potentials 1*A* and 2*A*, fitted to the *ab initio* points of Drucker *et al.* The states are labelled (j,L,J).

ever, all the plausible potentials gave predictions of the $R(2)$ and $Q(2)$ lines within 0.4 and 2.5 GHz of the experimental lines at 105.8 and 101.2 GHz respectively, so the $R(2)$ line and the difference between the $R(2)$ line and $Q(2)$ line were included in the subsequent fit.

With the extended data set (five frequencies and three values of eq_JQ), it proved possible to determine five parameters of potential form 1: ϵ_0, ϵ_2, R_{m0}, R_{m2} and β. The set chosen is of course somewhat arbitrary, though it could not be made any bigger with the present data set without introducing unacceptable correlations: We chose to float ϵ_2 and R_{m2} instead of ϵ_1 and R_{m1} because the even-order terms are generally better determined from spectroscopic data: in the limiting case of a free internal rotor model for the complex, odd-order Legendre terms in the potential have no diagonal matrix elements.

The optimised values of the parameters are given in Table III and a contour plot of the potential is shown in Figure 3. We designate this potential $1E8$ (where the $E8$ indicates that it was fitted to eight experimental data). The comparison between the observed and calculated spectroscopic properties is given in Table V, together with predictions for some other transitions that have not yet been observed. The complete energy level pattern for this potential, with predicted quadrupole coupling constants, is given in Figure 4.

TABLE V. Comparison of experimental and fitted results, all in MHz, except for well depth in cm^{-1}.

Assignment	Observed	Potential $1A8$	Potential $1E8$	Potential $2E8$
$(j,L,J)=(0,1,1)\leftarrow(0,0,0)$	15 893.6108(41)	14 618.7633	15 893.6125	15 893.6526
$24D_J$	461.9773	414.8900	461.9825	461.9225
$(j,L,J)=(1,1,2)\leftarrow(0,1,1)$	101 432.0812(67)	100 018.2316	101 432.1050	101 432.2675
$(j,L,J)=(1,2,3)\leftarrow(0,2,2)$	105 795.311	102 777.0209	105 795.0313	105 794.8725
$(j,L,J)=(1,2,3)\leftarrow(1,2,2)$	4604.2	−708.63	4 604.42	4 604.40
$(j,L,J)=(1,0,1)\leftarrow(0,0,0)$			98 603(12)	98 662(17)
$(j,L,J)=(1,1,1)\leftarrow(0,1,1)$			97 892(13)	98 076(19)
$(j,L,J)=(0,3,3)\leftarrow(0,2,2)$			45 767(12)	45 779(17)
$(j,L,J)=(1,3,3)\leftarrow(0,3,3)$			106 633(32)	106 173(36)
$eq_JQ(j,L,J)=(0,1,1)$	0.1118(15)	0.127	0.115	0.119
$eq_JQ(j,L,J)=(0,2,2)$	0.199(12)	0.216	0.211	0.215
$eq_JQ(j,L,J)=(1,1,2)$	0.7511(92)	0.8010	0.7822	0.7728
Well depth		25.06	29.47	29.36

The global minimum of potential $1E8$ is at the linear He–H–C–N configuration and has a depth 29.6 cm^{-1}. With only five parameters floating, the statistical uncertainty (95% confidence limits) in the absolute well depth is only 0.1cm^{-1}. However, this uncertainty is unrealistically low, and does not take model-dependence into account. A better estimate of the uncertainty may be obtained by calculating the Jacobian matrix (i.e., the matrix of partial derivatives of the observables with respect to the potential parameters) in a larger parameter space and repeating the statistical analysis. If we include the extra parameters R_{m1} and R_{m3} then the uncertainty increases to 4 cm^{-1}. Alternatively, if ϵ_1 and ϵ_3 are included with R_{m1} and R_{m3} fixed, the uncertainty increases to 8 cm^{-1}.

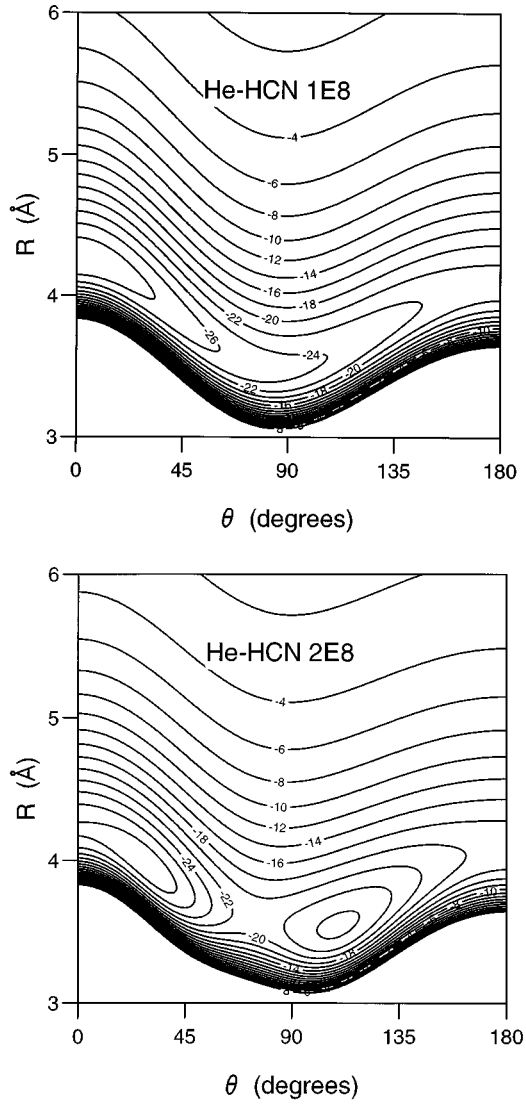

FIG. 3. Contour plots of the two potentials $1E8$ and $2E8$ fitted to the experimental data. The contour values are in cm^{-1}.

Despite the uncertainties, it seems that the true value of the absolute well depth is significantly larger than that obtained by Drucker *et al.*, which is 25.3 cm^{-1}. The discrepancy is slightly more than might have been expected from previous Møller–Plesset supermolecule calculations using bond-centered basis functions. Accordingly, we felt it desirable to repeat the fit with a different functional form, with somewhat more sophisticated representations of the repulsion and dispersion interactions. It was for this reason that we developed form 2 for the potential, which has the major advantage that a five-parameter potential can be determined from the experimental data without needing to fix any parameters at values from the supermolecule calculations.

As in the fit to the *ab initio* results, the parameters floated for form 2 were the repulsion scaling factor K_ρ, the positions of the two dispersion sites δ_A and δ_B, and the C_8/C_6 ratios τ_A and τ_B. The resulting potential is designated potential $2E8$. Its parameters are compared with those of the *ab initio* potential $2A$ in Table IV and a contour plot is shown in Figure 3. The complete energy level pattern for this potential is also shown in Figure 4. Comparisons with experimental results and spectroscopic predictions are given in Table V.

V. DISCUSSION

The functions $\epsilon(\theta)$ and $R_m(\theta)$ for the fitted potentials $1E8$ and $2E8$ are compared with values from the *ab initio* calculations of Drucker *et al.*[13] in Figure 5. It may be seen that the $R_m(\theta)$ functions are reasonably similar for the two

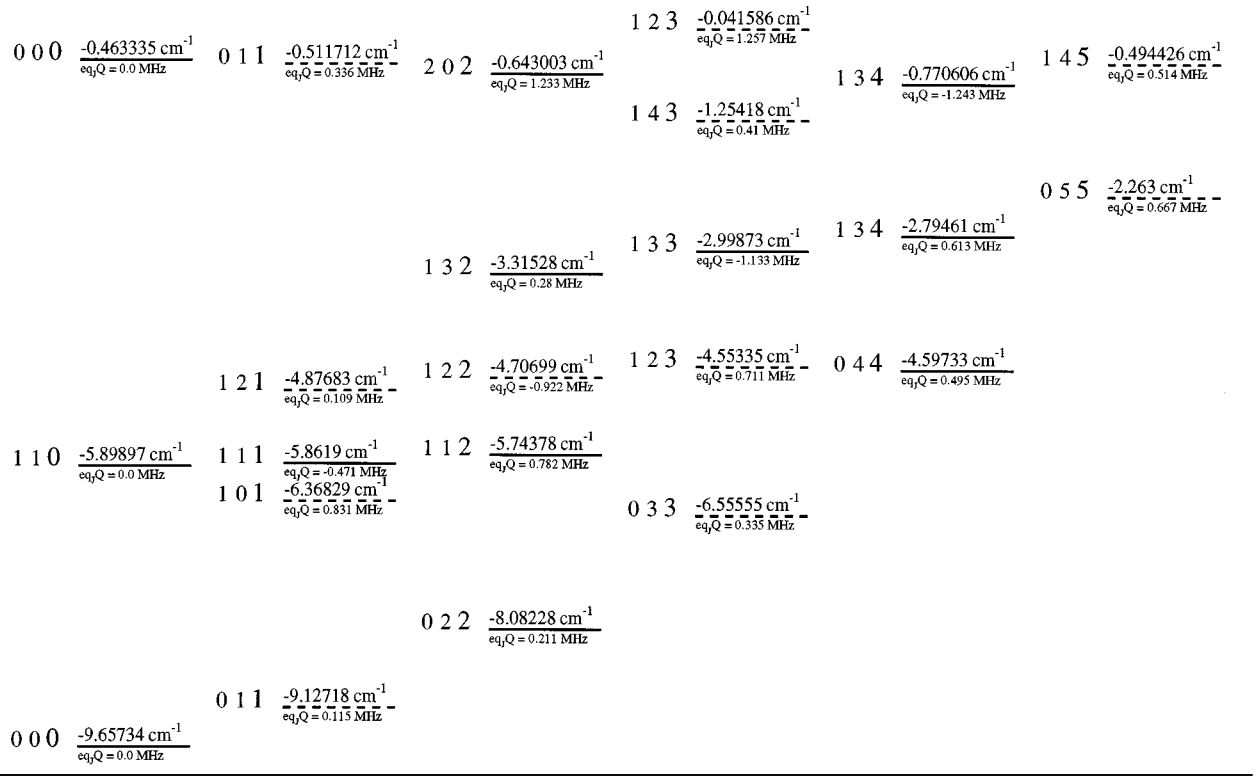

FIG. 4. The bound-state energies and quadrupole coupling constants for potentials $1E8$ (top) and $2E8$ (bottom) fitted to the experimental data. The states are labelled (j,L,J). The high-lying (0, 0, 0), (0, 1, 1) and (2, 0, 2) states in the $1E8$ potential correspond to excited van der Waals stretching states $n = 1$.

potentials, but the $\epsilon(\theta)$ functions are markedly different: Potential $2E8$ shows a marked oscillation in well depth with θ with a slightly non-linear equilibrium geometry, whereas potential $1E8$ is much smoother and is linear at equilibrium. Although the oscillations at first sight look surprising, their existence cannot be ruled out altogether: The *ab initio* calculations were not carried out on a dense enough angular grid to be sure that they would have been seen. Potential $1E8$ did not have the flexibility to develop such oscillations, as only one Legendre component of the well depth anisotropy (ϵ_2) was fitted to the experimental data. Nevertheless, on the whole it seems likely that the oscillations are an artefact of

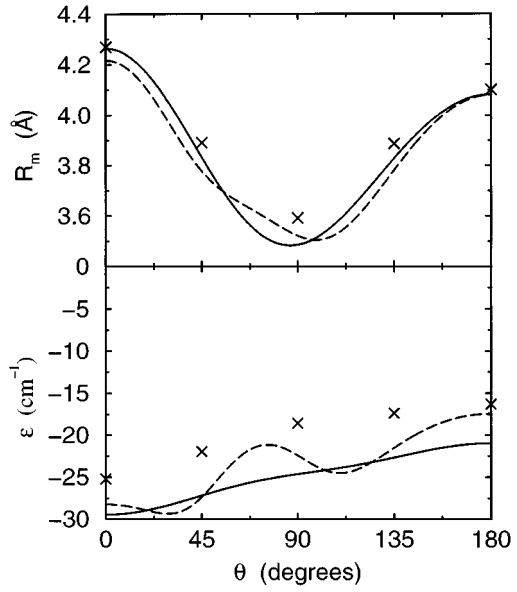

FIG. 5. The functions of $R_m(\theta)$ (position of the energy minimum), and $\epsilon(\theta)$ (well depth) ——: potential $1E8$, - - - -: potential $2E8$, × : results of Drucker *et al.*

distributing the dispersion interaction to only two sites within the HCN molecule: the two angular minima in potential $2E8$, at around 30° and 110°, are approximately at the angles where it is possible to approach the dispersion sites most closely. In any case, it must be concluded that the existing experimental data are not adequate to determine the well depth function in any detail. The equilibrium geometry is probably linear, He–H–C–N, but a slight non-linearity cannot be ruled out.

A major point of agreement between the two fitted potentials is that the well depth is significantly greater (by 3 to 5 cm^{-1}) than in the *ab initio* calculations of Drucker *et al.* The *ab initio* calculations appear to be quite accurate for R_m at the linear geometries, though they overestimate it for bent geometries.

Figure 6 shows the value of C_8 for each of the two fitted potentials as a function of θ. For potential $2E8$, $C_8(\theta)$ was calculated by re-expanding the potential about a single site (at the HCN center of mass), including contributions from the shifted C_6 coefficients. It is clear that potential $2E8$ has a much smaller C_8 coefficient than potential $1E8$, especially near the linear geometries. The values of C_8 for potential $2E8$ are physically more acceptable than those for potential $1E8$: For potential $2E8$, the value of C_8/C_6 at the linear geometries is about 60 a_0^2, which seems physically sensible, while for potential $1E8$ the ratio reaches over 180 at the linear He–H–C–N geometry. This unphysical behaviour probably arises because, for form 1, C_8 has to adjust excessively to compensate for deficiencies in the representation of other parts of the potential.

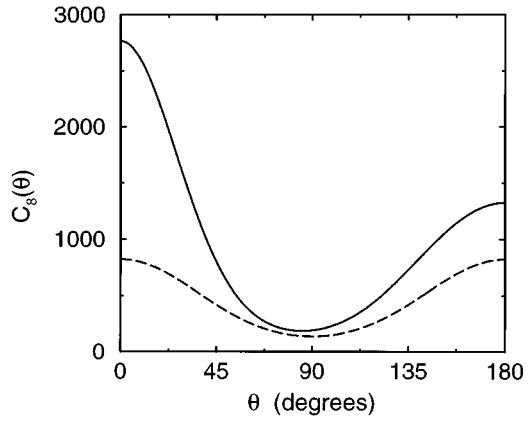

FIG. 6. The angular dependence of C_8 for the two potentials fitted to experimental data. ——: potential $1E8$, - - - -: potential $2E8$.

VI. CONCLUSIONS

We have obtained two potentials for He–HCN by fitting to rather limited experimental data from high-resolution microwave and millimeter-wave spectroscopy on the van der Waals complex. The fits made full use of both line positions and nuclear quadrupole coupling constants eq_JQ; indeed, the hyperfine-free line positions by themselves would not have been adequate to obtain satisfactory fitted potentials. During the fitting process, it became possible to assign some spectroscopic lines that had not previously been assignable.

The two fitted potentials use quite different functional forms. In the first, the well depth $\epsilon(\theta)$ and the position of the minimum $R_m(\theta)$ are each expanded as Legendre series in the angle θ. In fitting this potential, it was necessary to fix some parameters at values determined from the *ab initio* supermolecule calculations of Drucker *et al.* The second functional form is independent of the supermolecule calculations: it uses a repulsive wall based on monomer charge density calculations, and a two-site representation of the dispersion energy constrained to have the correct long-range C_6 and C_7 coefficients.

The fitted potentials both reproduce the experimental data to an accuracy of better than 1 MHz for rotational line frequencies and within 7% in the case of eq_JQ values. However, there are significant differences between the two potentials, especially in the shape of the well depth function $\epsilon(\theta)$. We have made predictions of the location of new, as yet unobserved, lines using both potentials. If these lines can be observed experimentally, further refinement of the potential will be possible.

ACKNOWLEDGMENTS

We would like to acknowledge the help of Dr. Mark Law for his help in the use of the I-NoLLS program and Dr. Richard Wheatley for his help in the use of the GMUL program. This work was supported by the Engineering and Physical Sciences Research Council through Collaborative Computational Project No. 6, on Heavy Particle Dynamics. The calculations were carried out on a cluster of IBM RS/6000 workstations belonging to the Atomic and Molecular

Physics groups at the Universities of Durham and Newcastle, and we are grateful to Dr. Lydia Heck for her assistance in this context.

[1] R. J. Le Roy and J. M. Hutson, J. Chem. Phys. **86**, 837 (1987).
[2] J. M. Hutson, J. Chem. Phys. **96**, 6752 (1992).
[3] J. M. Hutson, J. Phys. Chem. **96**, 4237 (1992).
[4] R. C. Cohen and R. J. Saykally, J. Chem. Phys. **98**, 6007 (1993).
[5] C. A. Schmuttenmaer, R. C. Cohen, and R. J. Saykally, J. Chem. Phys. **101**, 146 (1994).
[6] J. M. Hutson, A. Ernesti, M. M. Law, C. F. Roche, and R. J. Wheatley (unpublished).
[7] M. Quack and M. Suhm, J. Chem. Phys. **95**, 28 (1991).
[8] M. J. Elrod and R. J. Saykally, J. Chem. Phys. **103**, 933 (1995).
[9] C. M. Lovejoy and D. J. Nesbitt, J. Chem. Phys. **93**, 5387 (1990).
[10] M. J. Weida, J. M. Sperhac, D. J. Nesbitt, and J. M. Hutson, J. Chem. Phys. **101**, 8351 (1994).
[11] A. R. W. McKellar, J. Chem. Phys. **93**, 18 (1990).
[12] R. J. Le Roy C. Bissonnette, T. H. Wu, A. K. Dham, and W. J. Meath, Faraday Discuss. Chem. Soc. **97**, 81 (1994).
[13] S. Drucker, F.-M. Tao, and W. Klemperer, J. Phys. Chem. **99**, 2646 (1995). The line at 101.2 GHz has been more precisely measured at 101 191.09 MHz (private communication).
[14] A. Ernesti and J. M. Hutson, J. Chem. Phys. **101**, 5438 (1994).
[15] J. M. Hutson, Mol. Phys. **84**, 185 (1995).
[16] A. D. Buckingham, Adv. Chem. Phys. **12**, 107 (1967).
[17] C. Degli Esposti, G. Cazzoli, and P. G. Favero, Infrared Phys. **28**, 21 (1988).
[18] The quadrupole moment (relative to the center of mass) was obtained from an MP2 computation using the same basis set as for the frequency-dependent polarizability calculations.
[19] P. W. Fowler, Ann. Rep. Chem. Soc. C **84**, 3 (1987).
[20] R. D. Amos, and J. E. Rice, CADPAC: The Cambridge Analytical Derivatives Package, Issue 5 (1992).
[21] P. W. Fowler and G. H. F. Diercksen, Chem. Phys. Lett. **167**, 105 (1990).
[22] A. Koide, W. J. Meath, and A. R. Allnatt, J. Phys. Chem. **86**, 1222 (1982).
[23] J. M. Hutson, J. Chem. Phys. **89**, 4550 (1988).
[24] J. M. Hutson, J. Chem. Phys. **91**, 4448 (1989).
[25] J. M. Hutson, J. Chem. Phys. **91**, 4455 (1989).
[26] K. T. Tang and J. P. Toennies, J. Chem. Phys. **80**, 3726 (1984).
[27] R. J. Wheatley and S. L. Price, Mol. Phys. **71**, 1371 (1990).
[28] R. J. Wheatley, GMUL computer program (1995).
[29] *NAG FORTRAN Library*, *Mark 16* (Numerical Algorithms Group, Oxford, 1993).
[30] C. Douketis, J. M. Hutson, B. J. Orr, and G. Scoles, Mol. Phys. **52**, 763 (1984).
[31] J. M. Hutson, Adv. Mol. Vibrat. Coll. Dyn. A **1**, 1 (1991).
[32] C. H. Townes and A. L. Schawlow, *Microwave Spectroscopy* (Mc-Graw Hill, New York, 1955).
[33] R. C. Cohen and R. J. Saykally, J. Phys. Chem. **94**, 7991 (1990).
[34] J. M. Hutson, BOUND computer program, version 5, distributed by Collaborative Computational Project No. 6 of the UK Science and Engineering Research Council (1993).
[35] J. M. Hutson, Comput. Phys. Commun. **84**, 1 (1994).
[36] F. DeLucia and W. Gordy, Phys. Rev. **187**, 58 (1969).
[37] B. R. Johnson, J. Chem. Phys. **69**, 4678 (1978).
[38] M. M. Law and J. M. Hutson, I-NoLLS computer program (1996).